UAV-Enabled Integrated Sensing, Computing and Communication for Internet of Things: Joint Resource Allocation and Trajectory Design

Yige Zhou, Xin Liu, *Senior Member, IEEE,* Xiangping Zhai, *Member, IEEE,* Qiuming Zhu, *Senior Member, IEEE,* and Tariq S Durrani, *Life Fellow, IEEE*

***Abstract*—As an aerial service platform for Internet of Things (IoT), unmanned aerial vehicle (UAV) can provide integrated sensing, computing and communication (ISCAC) services for the IoT nodes. In this paper, a UAV-enabled ISCAC system is proposed for IoT to meet the evolving requirements of emerging services in 6G networks. This system has three functions: sensing user equipments (UEs) for acquiring radar sensing information, executing computing tasks, and offloading incomplete tasks to the access point (AP) for further processing. Through jointly optimizing UAV CPU frequency, UAV radar sensing power, transmit power of UEs, and UAV trajectory, the weighted total energy consumption of both the UAV and the UEs can be minimized. We present a three-layer iterative optimization algorithm to tackle the original non-convex optimization problem. Finally, the effectiveness of the algorithm and its superiority in energy consumption compared to other benchmark schemes are verified through simulation results.**

***Index Terms*—UAV, IoT, resource allocation, trajectory optimization.**

I. Introduction

Internet of Things (IoT) aims to connect Internet with various objects, forming a complete network system. And the IoT finds extensive applications across diverse sectors, such as healthcare, transportation, agriculture, etc [1] [2]. However, in some special scenarios, such as remote areas where the terrain is not suitable for deploying communication infrastructure, the IoT user equipments (UEs) cannot send their sensing data to the data center, and the data center is also unable to obtain the status of the UEs. Recently, the utilization of unmanned aerial vehicles (UAVs) to aid ground communications has seen extensive adoption, primarily owing to their affordability, adaptable mobility, rapid deployment capabilities, and the availability of line-of-sight (LoS) connections [3] [4] [5]. The use of UAVs as relays to enhance ground IoT communications effectively solves the above problems. The UAV-enabled integrated sensing and communications (ISAC) system can sense and communicate with the IoT UEs as well as forward the sensing data and communication information to the data center. However, the UAV may achieve a large amount of intricate data that cannot be processed effectively. The UAV-enabled mobile edge computing (MEC) system deploys a powerful MEC server on the UAV to provide computing services for both radar sensing data and communication data uploaded by the IoT UEs, greatly reducing energy consumption and transmit delay. Therefore, the integration of sensing, computing, and communication (ISCAC) is regarded as a promising technology for enhancing the performance of UAVs in serving IoT [6].

The use of UAVs to enable ISAC has attracted substantial interest from both the academic and industrial sectors [7] [8] [9]. In [10], Jiang *et al.* proposed a UAV swarm network that leverages extended kalman filter algorithm to enhance target sensing accuracy. Additionally, the UAV communication delay was reduced by proposing identification friend or foe method. In [11], Zhang *et al.* designed a UAV-aided ISAC network, whose peak Age of Information (AoI) was minimized through optimizing UAV trajectory, scheduling order, and power/time allocation for sensing and communication tasks. Wan *et al.* developed a joint channel estimation and radar sensing algorithm for the UAV-ISAC networks with millimeter-wave (mmWave) massive multiple-input multiple-output (mMIMO) [12]. And compressed sensing technology was used to achieve the integration of channel estimation and radar sensing with low pilot overhead. In [13], Zhao *et al.* proposed a UAV communication model with jitter effect. By utilizing an ISAC based channel estimation method, the UAV sensing, data transmission and UAV control are integrated to improve the system performance. In [14], Zhong *et al.* placed a uniform linear array (ULA) vertically on the UAV, and the UAV performs ISAC tasks, communicates with multiple users, and simultaneously senses ground targets. Considering both stationary and mobile scenarios, the UAV's throughput was maximized by jointly designing maneuver and beamforming, while ensuring radar sensing requirements. In [15], Salem *et al.* considered security issues for a reconfigurable intelligent surface (RIS) enabled UAV-ISAC system when being eavesdropped by a malicious UAV. By jointly designing radar receiving beamformer, active RIS reflection coefficient matrix and transmitting beamformer, the achievable system secrecy

Manuscript received xx, xxxx; revised August xx, xxxx. (*Correspondence author: Xin Liu*)

Yige Zhou and Xin Liu are with the School of Information and Communication Engineering, Dalian University of Technology, Dalian 116024, China (e-mail: zhouyg2022@mail.dlut.edu.cn; liuxinstar1984@dlut.edu.cn).

Xiangping Zhai is with the College of Computer Science and Technology, Nanjing University of Aeronautics and Astronautics, Nanjing 211106, China (e-mail: blueicezhaixp@nuaa.edu.cn).

Qiuming Zhu is with the Key Laboratory of Dynamic Cognitive System of Electromagnetic Spectrum Space, College of Electronic and Information Engineering, Nanjing University of Aeronautics and Astronautics, Nanjing 211106, China (e-mail: zhuqiuming@nuaa.edu.cn).

T. S. Durrani is with the Department of Electronic and Electrical Engineering, University of Strathclyde, Glasgow G1 1XQ, U.K. (e-mail: t.durrani@strath.ac.uk).

This is a peer-reviewed, accepted manuscript of the following paper: Zhou, Y., Liu, X., Zhai, X., Zhu, Q., & Durrani, T. S. (2024). UAV-enabled integrated sensing, computing, and communication for Internet of Things: joint resource allocation and trajectory design. IEEE Internet of Things Journal, 11(7), 12717-12727. https://doi.org/10.1109/JIOT.2023.3335937

rate was maximized. In [16], Liu *et al.* introduced radar mutual information (MI) to measure radar detection performance of UAV-ISAC system. By jointly optimizing task scheduling, transmit power, and UAV trajectory, the energy efficiency (EE) of the system was maximized while guaranteeing sensing fairness. In [17], Ning *et al.* presented a multi-UAV trajectory optimization algorithm to execute flying actions distributively based on partial information. To the best of our knowledge, this is the first work to realize distributed multi-UAV trajectory control in multi-SP scenarios with probabilistic time-varying service preferences. In [18], Qin *et al.* proposed a multi-UAV enable mobile ISAC platforms for both sensing and communication with target users. To maximize the minimum spectral efficiency among the UAVs, deep reinforcement learning (DRL) was adopted to optimize user association, UAV trajectory and transmit power.

The UAV-enabled MEC has also attracted great interests among researchers [19] [20], which can provide computing assistance to ground users in scenarios where there is no MEC server available on the ground. In [21], Wang *et al.* proposed a UAV-enabled MEC network to provide computing services for randomly distributed mobile devices, and the UAV energy consumption was significantly reduced by region partitioning and UAV trajectory optimization. In [22], Li *et al.* focused on maximizing the UAV EE by jointly optimizing UAV trajectory, user transmit power, and computation load allocation. In [23], Zhang *et al.* proposed a UAV-enabled MEC system based on NOMA, and minimized the energy consumption of multiple UAVs and terrestrial users. In [24], Asim *et al.* designed a multi-IRS and multi-UAV assisted MEC system, and the overall system cost including energy consumption, completion time, and maintenance cost of UAVs was minimized by proposing a four-stage algorithm to jointly optimize UAVs trajectories and IRSs phase shifts. In [25], Lu *et al.* tried to maximize the security calculating efficiency of a UAV-aided MEC network by employing DRL to optimize the offloading decisions and resource allocations. In addition, the UAV could also serve as a relay to help users effectively transfer their computing tasks to remote MEC servers [26] [27]. Many works have focused on differentiated services of service providers, but are not suitable for UAV networks due to their unique service providers. As far as we know, [28] is the first work to investigate differentiated services for the UAV network with distinct service providers. In [26], Zhang *et al.* presented a joint optimization algotihm of bit allocation, time slot scheduling, transmit power and UAV trajectory to minimize energy consumption of communication, computation, and UAV flight. In [27], Liu *et al.* proposed a three-stage iterative optimization algorithm to minimize the total energy consumption of UAV-assisted MEC network by optimizing parameters of UAVs and UEs.

At present, there is relatively less literature for UAV enabled ISCAC. In [29], Huang *et al.* proposed a UAV-ISAC aided MEC system, however, ignoring the task computing ability of the UAV itself, the UAV has to offload the radar sensing data to the edge-server of the base station (BS) for further processing. In [30], Xu *et al.* proposed a UAV-enabled ISCAC framework, and achieved a balance between computing capacity and sensing beampattern gain by optimizing beamforming vector and UAV trajectory. However, the UAV energy consumption was not explicitly addressed. In this paper, we propose a UAV-enabled ISCAC model for ground IoT, and seek to minimize the weighted total energy consumption of both UAV and UEs. The contributions of this paper are summarized as follows.

- A UAV-enabled ISCAC model is established, where the UAV performs three essential functions: sensing UEs for acquiring radar detection information, executing computing tasks, and offloading incomplete tasks to the access point (AP) for further processing. We formulate a joint optimization problem of UAV CPU frequency, UAV radar sensing power, UEs transmit power, and UAV trajectory to minimize the overall energy consumption of both the UAV and the UEs.
- The original optimization problem is non-convex in nature. To solve this problem, it is divided into two sub-optimization problems, resource allocation optimization and UAV trajectory optimization, each of which can be solved by proposing an iterative optimization algorithm based on successive convex approximation (SCA).

The remainder of this paper is structured as follows. In Section II, the system model is proposed, where the communication model, sensing model and computing model are described, respectively. In Section III, we formulate a joint resource allocation and UAV trajectory optimization problem, and propose iterative optimization algorithms to solve the problem. Some numerical simulation results are presented and analyzed in Section IV. In Section V, we finally conclude the paper.

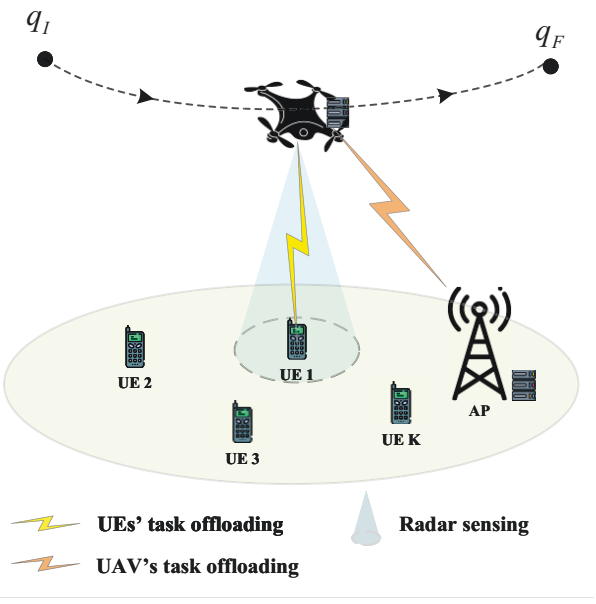

Fig. 1. System model.

II. System Model

In Fig. 1, we consider a UAV-enabled ISCAC system consisting of a single UAV, a ground AP, and K UEs. The UAV is

equipped with an ISAC device and a MEC server to simultaneously perform radar sensing, communication and computing. Specifically, the UAV ISAC device first emits radar sensing signals to obtain the sensing data of the UEs; considering the limited computing power of the UEs, they need to offload the task data that cannot be processed to the UAV; then, the UAV MEC server can simultaneously process radar sensing data and UEs computing tasks. In addition, considering the carrying capacity of the UAV and the performance requirements of the system, an AP with MEC server is established on the ground to assist the UAV computing. The UAV functions as a relay to offload unfinished computing tasks to the AP for further computations.

Define $\mathcal{K} = \{1, 2, ..., K\}$ as set of UEs. To facilitate the analysis, we uniformly divide the task completion time T into S time slots, and define $\mathcal{S} = \{1, 2, ..., S\}$ as the set of time slots. The time slot interval is $\delta_t = T/S$, which is selected to be small enough to guarantee that the UAV location is considered fixed within each time slot. Accordingly, in a three-dimensional Cartesian coordinate system, the coordinate of UAV in sth time slot is represented as $(q[s], H)$, where $q[s] = (x[s], y[s])$ and H denote the horizontal location and flight altitude of the UAV, respectively. The locations of the kth UE and AP are fixed and denoted as $u_k = (x_k, y_k)$ and $u_a = (x_a, y_a)$, respectively. The UAV flies from its initial position q_I to its final position q_F within a mission cycle T.

A. Communication Model

The reference [31] indicates that for a service area with a side length of 40m and a UAV flight altitude of 20m, the likelihood of achieving a LoS condition is close to 1. Hence, the channels between the UAV and the UEs as well as the AP are predominantly characterized by LoS links. Specifically, the channel power gains of the communication links between the UAV and the kth UE as well as the AP at the sth time slot are

$$h_k[s] = \frac{G_t G_c \lambda^2}{(4\pi)^2 d_k^2[s]} = \frac{\beta_{com}}{d_k^2[s]}, \forall s \tag{1}$$

$$h_a[s] = \frac{G_t G_c \lambda^2}{(4\pi)^2 d_a^2[s]} = \frac{\beta_{com}}{d_a^2[s]}, \forall s \tag{2}$$

where G_t and G_c denote the antenna gains of the UAV transmitter and communication receiver, respectively; $d_k[s]$ and $d_a[s]$ denote the distance from the UAV to the kth UE and the distance from the UAV to the AP, respectively; $\lambda = c/f_c$ indicates the signal wavelength, where c and f_c denote the speed of light and signal carrier frequency, respectively; $\beta_{com} = \frac{G_t G_c \lambda^2}{(4\pi)^2}$.

B. Sensing Model

Based on the scattering transmission characteristics of radar detection signal [32], [33], the channel power gain of the radar detection link between the UAV and the kth UE at the sth time slot is

$$h_{k,rad}[s] = \frac{G_t G_r \lambda^2 \sigma}{(4\pi)^3 d_k^4[s]} = \frac{\beta_{rad}}{d_k^4[s]}, \forall s \tag{3}$$

where G_r denotes the antenna gain of UAV radar receiver, σ denotes radar cross-section (RCS) of target, and $\beta_{rad} = \frac{G_t G_r \lambda^2 \sigma}{(4\pi)^3}$.

C. Computing Model

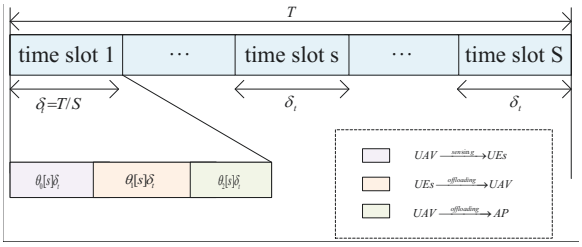

Fig. 2. Time slot division.

To avoid interference, the ground UEs use TDMA to access the UAV. Note that the delay and energy consumption for sending computing results back from the UAV to UEs, as well as from the AP to the UAV, can be omitted by considering that the size of results is significantly smaller than that of the offloaded data.

As illustrated in Fig. 2, each time slot is further divided into three sub-time slots. The first sub-time slot $\theta_0[s]$ is dedicated to the UAV sensing the UEs, the second sub-time slot $\theta_1[s]$ involves the UEs offloading all their tasks to the UAV, and the third sub-time slot $\theta_2[s]$ is allocated for the UAV to offload a portion of the tasks to the AP. Obviously, the length of sub-time slots satisfies

$$\theta_0[s] + \theta_1[s] + \theta_2[s] = 1 \tag{4}$$

1) UAV's Sensing Data Acquisition: We utilize radar estimation rate to measure the radar detection performance. The radar estimation rate of the UAV sensing the kth UE at the sth time slot is

$$R_{k,rad}[s] = B\log_2\left(1 + \frac{p_{k,d}[s] h_{k,rad}[s]}{\sigma_u^2}\right), \forall k, s \tag{5}$$

where $p_{k,d}[s]$ denotes the sensing power of the UAV to the kth UE, σ_u^2 denotes the noise power, and B denotes the communication bandwidth.

The sub-time slot for sensing is further divided into K equal time intervals for UEs, ensuring that each UE is sensed in the different time intervals. Therefore, the number of sensing bits and the corresponding UAV energy consumption for the kth UE in the sth time slot are

$$l_{k,rad}[s] = \theta_0[s] \frac{\delta_t}{K} R_{k,rad}[s] \tag{6}$$

$$E_{k,rad}[s] = p_{k,d}[s] \theta_0[s] \frac{\delta_t}{K} \tag{7}$$

2) UEs' Computation Offloading: The offloading rate of the kth UE at the sth time slot is expressed as

$$R_{k,off}[s] = B\log_2\left(1 + \frac{p_k[s] h_k[s]}{\sigma_u^2}\right), \forall k, s \tag{8}$$

where $p_k[s]$ denotes the transmit power of the kth UE. The sub-time slot for computation offloading is further divided into

K equal time intervals, allocated to the K UEs for offloading. Therefore, the number of offloading bits and the corresponding energy consumption for the kth UE are

$$l_{k,off}[s] = \theta_1[s]\frac{\delta_t}{K}R_{k,off}[s] \tag{9}$$

$$E_{k,off}[s] = p_k[s]\theta_1[s]\frac{\delta_t}{K} \tag{10}$$

Once all the UEs have finished computation offloading in each time slot, the UAV will continue to perform the computing tasks. The number of computation bits computed by the UAV for the kth UE in the sth time slot can be given as

$$l_{k,u}[s] = \frac{f_{k,u}[s]}{C_k}\theta_2[s]\delta_t, \forall k, s \tag{11}$$

where $f_{k,u}[s]$ denotes the UAV CPU frequency allocated to the kth UE. Therefore, the energy consumption for UAV computing in each time slot is

$$E_{k,u}[s] = k_u(f_{k,u}[s])^3\theta_2[s]\delta_t, \forall k, s \tag{12}$$

where k_u denotes the effective capacitance coefficient of the UAV processors, which is a constant determined by the hardware specifications of the UAV.

3) UAV's Computation Offloading: To maintain higher service quality for the UEs, the UAV can transfer some complex computational tasks to the AP for processing. To ensure that all the unprocessed task data is successfully offloaded to the AP, the transmit power of the UAV needs to satisfy

$$p_a[s] \geq \frac{\sigma_a^2}{h_a[s]}\left(2^{\frac{\sum_{k=1}^{K}(l_{k,rad}[s]+l_{k,off}[s]-l_{k,u}[s])}{B\theta_2[s]\delta_t}}-1\right), \forall s \tag{13}$$

Therefore, the UAV energy consumption for offloading tasks to the AP is

$$E_a[s] = p_a[s]\theta_2[s]\delta_t, \forall s \tag{14}$$

4) Flying Model: Assuming that the UAV flies at a uniform speed in a straight line within a single time slot, the UAV flight speed is

$$v[s] = \frac{q[s+1]-q[s]}{\delta_t}, \forall s \tag{15}$$

According to [34], the UAV propulsion power at the sth time slot is determined by

$$\begin{aligned} P(\|v[s]\|) = P_0\left(1+\frac{3\|v[s]\|^2}{U_{tip}^2}\right) + \frac{1}{2}d_0\rho_0 sA\|v[s]\|^3 \\ +P_H\left(\sqrt{1+\frac{\|v[s]\|^4}{4v_0^4}}-\frac{\|v[s]\|^2}{2v_0^2}\right)^{\frac{1}{2}} \end{aligned} \tag{16}$$

where P_0 and P_H denote the blade profile power and induced power in hovering status, respectively; U_{tip} represents rotor tip velocity; v_0 represents the average blade induced velocity during hover; d_0, ρ_0, s_0 and A denote fuselage drag ratio, air resistance, rotor stability and rotor disc area, respectively. The UAV's flight energy consumption in each time slot is

$$E_f[s] = P(\|v[s]\|)\delta_t \tag{17}$$

Therefore, the total UAV energy consumption for sensing, computing, offloading, and flight is

$$E_{uav}[s] = \sum_{k=1}^{K}(E_{k,rad}[s]+E_{k,u}[s]) + E_a[s] + E_f[s] \tag{18}$$

Furthermore, the total energy consumption of all the UEs is

$$E_{user}[s] = \sum_{k=1}^{K}E_{k,off}[s] \tag{19}$$

III. Resource Allocation and UAV Trajectory Design

A. Problem Formulation

We seek to minimize the weighted total energy consumption of all the UEs and the UAV in each time slot. Since the energy consumption of the UEs is often smaller than that of the UAV, we use a weight factor to balance the energy consumption of the UAV and UEs. The optimization problem is given by

$$\min_{\mathbf{L}[s],\mathbf{q}[s]} E_{user}[s] + \eta E_{uav}[s] \tag{20a}$$

$$\text{s.t.} \quad l_{k,u}[s] \leq l_{k,rad}[s] + l_{k,off}[s], \forall k, s \tag{20b}$$

$$0 \leq p_k[s] \leq p_{l,\max}, \forall k, s \tag{20c}$$

$$0 \leq f_{k,u}[s], \forall k, s \tag{20d}$$

$$\sum_{k=1}^{K} f_{k,u}[s] \leq f_{u,\max}, \forall s \tag{20e}$$

$$0 \leq p_{k,d}[s] \leq p_{d,\max}, \forall k, s \tag{20f}$$

$$0 \leq \frac{\sigma_a^2}{h_a[s]}\left(2^{\frac{\sum_{k=1}^{K}(l_{k,rad}[s]+l_{k,off}[s]-l_{k,u}[s])}{B\theta_2[s]\delta_t}}-1\right) \leq p_{u,\max}, \forall s \tag{20g}$$

$$\|q[s]-q[s-1]\| \leq v_{\max}\delta_t, \forall s \tag{20h}$$

$$q[0] = q_I, q[S+1] = q_F \tag{20i}$$

$$\|q[s]-q_F\| \leq (S-s+1)v_{\max}\delta_t, \forall s \tag{20j}$$

where $\mathbf{L}[s] = \{f_{k,u}[s], p_{k,d}[s], p_k[s]\}$ and $\theta[s] = \{\theta_0[s], \theta_1[s], \theta_2[s]\}$ denote the resource allocation and time slot scheduling, respectively; η denotes the weight factor. (20b) ensures that the the number of computing bits performed by the UAV does not exceed the sum of UAV sensing bits and UE offloading bits. (20c) denotes the upper limit imposed on the transmit power of the UEs in adherence to the power constraint. (20d)-(20g) are the relevant parameter constraints for the UAV operation. Specifically, (20d) and (20e) delineate the upper limits of the achieved UAV CPU frequency; (20f) represents the maximum sensing power devoted to radar sensing tasks by the UAV; (20g) ensures that the UAV can offload the incomplete tasks to the AP. (20h) represents the maximum flight speed constraint of the UAV. (20i) denotes the constraint of starting and ending points of the UAV flight. (20j) ensures that the UAV can reach the ending point at the $(S+1)$th time slot.

Due to the non-convexity of the objective function and the constraints (20b), (20g), directly solving the optimization

problem becomes challenging. Consequently, we divide the original optimization problem into two subproblems, resource allocation optimization and UAV trajectory optimization, each of which can be solved by the SCA.

B. Resource Allocation Optimization

Assuming that the UAV trajectory is fixed, the resource allocation optimization subproblem is given by

$$\min_{\mathbf{L}[\boldsymbol{s}]} E_{user}[s] + \eta E_{uav}[s] \tag{21a}$$

$$\text{s.t.} \quad (20b) - (20g) \tag{21b}$$

To solve this subproblem, we propose a three-layer iterative optimization algorithm to jointly optimize the UAV CPU frequency, UAV radar sensing power, and UEs transmit power.

1) UAV CPU Frequency Optimization: Firstly, the optimization problem concerning the UAV CPU frequency $f_{k,u}[s]$ under the condition of fixed UAV sensing power $p_{k,d}[s]$ and UEs transmit power $p_k[s]$ can be given by

$$\min_{f_{k,u}[s]} \gamma_0(\mathbf{L}[\boldsymbol{s}], \mathbf{q}[s]) \tag{22a}$$

$$\text{s.t.} \quad (20b), (20d), (20e), (20g) \tag{22b}$$

The specific expression for optimization objective γ_0 is provided in (22) and can be found at the bottom of the next page. And this is a convex optimization problem that can be directly solved by the CVX.

2) UAV Rader Sensing Power Optimization: With the fixed UEs transmit power $p_k[s]$ and UAV CPU frequency $f_{k,u}[s]$, the allocation problem of UAV sensing power $p_{k,d}[s]$ can be given by

$$\min_{p_{k,d}[s]} \gamma_0(\mathbf{L}[\boldsymbol{s}], \mathbf{q}[s]) \tag{23a}$$

$$\text{s.t.} \quad (20b), (20f), (20g) \tag{23b}$$

Given that both the objective function (23a) and the constraints (20b), (20g) are all non-convex, it is evident that (23) is non-convex. The SCA method can be adopted to solve the problem, which allows us to transform the non-convex problem (23) into a convex problem. For any local point $p^r_{k,d}[s]$, $R_{k,rad}[s]$ can be replaced by its first-order Taylor expansion as follows

$$\begin{aligned} R^s_{k,rad}[s] &= B\log_2\left(1+\frac{p^r_{k,d}[s]h_{k,rad}[s]}{\sigma_u^2}\right) \\ &+\frac{Bh_{k,rad}[s]}{\ln 2\left(\sigma_u^2+p^r_{k,d}[s]h_{k,rad}[s]\right)}\left(p_{k,d}[s]-p^r_{k,d}[s]\right) \end{aligned} \tag{24}$$

Therefore, problem (23) can be rewritten as

$$\min_{p_{k,d}[s]} \gamma_1(\mathbf{L}[\boldsymbol{s}], \mathbf{q}[s]) \tag{25a}$$

$$\text{s.t.} \quad R^s_{k,rad}[s] + \frac{\theta_1[s]}{\theta_0[s]} R_{k,off}[s] \geq \frac{K\theta_2[s]f_{k,u}[s]}{\theta_0[s]C_k} \tag{25b}$$

$$0 \leq p_{k,d}[s] \leq p_{d,\max}, \forall k, s \tag{25c}$$

$$\begin{aligned} &\sum_{k=1}^{K} R^s_{k,rad}[s] + \tfrac{\theta_1[s]}{\theta_0[s]} \sum_{k=1}^{K} R_{k,off}[s] \leq \\ &\tfrac{KB\theta_2[s]}{\theta_0[s]}\log_2\left(p_{u,\max}\tfrac{h_a[s]}{\sigma_a^2}+1\right) + \tfrac{K\theta_2[s]}{\theta_0[s]}\sum_{k=1}^{K}\tfrac{f_{k,u}[s]}{C_k} \end{aligned} \tag{25d}$$

where γ_1 is provided in (26) and can be found at the bottom of the next page. Certainly, (25) exhibits convexity and can be directly solved using the CVX.

3) UEs Transmit Power Optimization: Given the UAV CPU frequency $f_{k,u}[s]$ and the UAV sensing power $p_{k,d}[s]$, the optimization problem of UEs transmit power $p_k[s]$ can be given by

$$\min_{p_k[s]} \gamma_0(\mathbf{L}[\boldsymbol{s}], \mathbf{q}[s]) \tag{27a}$$

$$\text{s.t.} \quad (20b), (20c), (20g) \tag{27b}$$

Due to that the objective function (27a) and the constraints (20b), (20g) are all non-convex, problem (27) is also non-convex. Similarly, by the SCA method, we can convert (27) into a convex problem. Specifically, for a given local point $p^r_k[s]$, $R_{k,off}[s]$ can be replaced by its first-order Taylor expansion as

$$\begin{aligned} R^c_{k,off}[s] &= B\log_2\left(1+\tfrac{p^r_k[s]h_k[s]}{\sigma_u^2}\right) \\ &+\tfrac{Bh_k[s]}{\ln 2\left(\sigma_u^2+p^r_k[s]h_k[s]\right)}\left(p_k[s]-p^r_k[s]\right) \end{aligned} \tag{28}$$

Therefore, problem (27) can be rewritten as

$$\min_{p_{k,d}[s]} \gamma_2(\mathbf{L}[\boldsymbol{s}], \mathbf{q}[s]) \tag{29a}$$

$$\text{s.t.} \quad R^c_{k,off}[s] + \frac{\theta_0[s]}{\theta_1[s]} R_{k,rad}[s] \geq \frac{K\theta_2[s]f_{k,u}[s]}{\theta_1[s]C_k} \tag{29b}$$

$$0 \leq p_k[s] \leq p_{l,\max}, \forall k, s \tag{29c}$$

$$\begin{aligned} &\sum_{k=1}^{K} R^c_{k,off}[s] + \tfrac{\theta_0[s]}{\theta_1[s]} \sum_{k=1}^{K} R_{k,rad}[s] \leq \\ &\tfrac{KB\theta_2[s]}{\theta_1[s]}\log_2\left(p_{u,\max}\tfrac{h_a[s]}{\sigma_a^2}+1\right) + \tfrac{K\theta_2[s]}{\theta_1[s]}\sum_{k=1}^{K}\tfrac{f_{k,u}[s]}{C_k} \end{aligned} \tag{29d}$$

where γ_2 is provided in (30) and can be found at the bottom of the next page. Obviously, (29) is convex and can be directly solved employing the CVX.

4) Three-Layer Iterative Optimization: Upon solving problems (22), (25), and (29), we derive the optimal solutions of the UAV CPU frequency $f_{k,u}[s]$, the UAV sensing power $p_{k,d}[s]$, and the UEs transmit power $p_k[s]$. To attain the optimal solution for (21), we put forward a three-layer iterative optimization algorithm as shown in Algorithm 1, which performs iterative optimization on $f_{k,u}[s]$, $p_{k,d}[s]$, and $p_k[s]$ until the objective function value converges.

C. UAV Trajectory Optimization

Using the solutions acquired from the resource allocation optimization subproblem as the initial values, the UAV trajectory optimization subproblem is represented as

$$\min_{\mathbf{q}[s]} \gamma_3(\mathbf{L}[\boldsymbol{s}], \mathbf{q}[s]) \tag{31a}$$

$$\text{s.t.} \quad (20b), (20g), (20h) - (20j) \tag{31b}$$

where γ_3 is provided in (32) and can be found at the bottom of the next page. The optimization problem is non-convex because of the non-convex objective function (31a) and the non-convex constraints (20b), (20g).

Algorithm 1 Three-layer iterative optimization

1: **Initialize**: the iteration index r=0, the UAV CPU frequency $f_{k,u}^r[s]$, the UAV sensing power $p_{k,d}^r[s]$, the UEs transmit power $p_k^r[s]$, and the tolerance error ε;
2: **repeat**
3: given $p_{k,d}^r[s]$ and $p_k^r[s]$, solve (22) to obtain $f_{k,u}^{r+1}[s]$;
4: given $f_{k,u}^r[s]$ and $p_k^r[s]$, solve (25) to obtain $p_{k,d}^{r+1}[s]$;
5: given $f_{k,u}^r[s]$ and $p_{k,d}^r[s]$, solve (29) to obtain $p_k^{r+1}[s]$;
6: $r = r + 1$;
7: **until** the target converges within the error of ε;
8: **Output**: the UAV CPU frequency $f_{k,u}[s]$, the UAV sensing power $p_{k,d}[s]$, the UEs transmit power $p_k[s]$.

According to [27], we first introduce the auxiliary variables $\tau = \{\tau_1[s], \tau_2[s]\}$ that satisfy

$$\tau_1[s] \geq \|v[s]\| \tag{33a}$$

$$\tau_2^2[s] \geq \sqrt{1 + \frac{\|v[s]\|^4}{4v_0^4}} - \frac{\|v[s]\|^2}{2v_0^2} \tag{33b}$$

Based on these two conditions, we can obtain

$$\tau_2^2[s] + \frac{\tau_1^2[s]}{v_0^2} \geq \frac{1}{\tau_2^2[s]} \tag{34}$$

As the left side of (34) is convex, we can replace it with its first-order Taylor expansion for any given local point $\{\tau_1^r[s], \tau_2^r[s]\}$. This approximation can be denoted as

$$\begin{aligned}\xi_1^r[s] &= \left(\tau_2^r[s]\right)^2 + 2\tau_2^r[s]\left(\tau_2[s] - \tau_2^r[s]\right) \\ &+ \tfrac{(\tau_1^r[s])^2}{v_0^2} + 2\tfrac{\tau_1^r[s]}{v_0^2}\left(\tau_1[s] - \tau_1^r[s]\right)\end{aligned} \tag{35}$$

Subsequently, we introduce the auxiliary variable $\beta_0[s]$ that satisfies

$$2^{\frac{\sum_{k=1}^{K}\left(l_{k,rad}[s]+l_{k,off}[s]-l_{k,u}[s]\right)}{B\theta_2[s]\delta_t}} \leq \beta_0[s] \tag{36a}$$

$$1 \leq \beta_0[s] \leq \beta_{0,\max}[s] \tag{36b}$$

where $\beta_{0,\max}[s]$ denotes the maximum value of $\beta_0[s]$, which is given by

$$\beta_{0,\max}[s] = \frac{\rho_{\max}}{\|q[s] - u_a\|^2 + H^2} + 1 \tag{37}$$

where $\rho_{\max} = \frac{p_{u,\max}\beta_{com}}{\sigma_a^2}$. Since (36a) is still non-convex, we proceed by introducing auxiliary variables $\beta_{1,k}[s], k = 1, 2, ..., K$ and $\beta_{2,k}[s], k = 1, 2, ..., K$ that satisfy

$$\log_2\left(1 + \frac{p_{k,d}[s]h_{k,rad}[s]}{\sigma_u^2}\right) \leq \beta_{1,k}[s] \tag{38}$$

$$\log_2\left(1 + \frac{p_k[s]h_k[s]}{\sigma_u^2}\right) \leq \beta_{2,k}[s] \tag{39}$$

After further scaling, (36a) is represented as

$$\begin{aligned}&\sum_{k=1}^{K}\left(\theta_0[s]\tfrac{\delta_t}{K}B\beta_{1,k}[s] + \theta_1[s]\tfrac{\delta_t}{K}B\beta_{2,k}[s] - \tfrac{f_{k,u}[s]}{C_k}\theta_2[s]\delta_t\right) \\ &\leq B\theta_2[s]\delta_t\log_2(\beta_0[s])\end{aligned} \tag{40}$$

By introducing the auxiliary variables $\beta_{3,k}[s], k = 1, 2, ..., K$, which satisfy

$$\beta_{3,k}[s] \leq (\|q[s] - u_k\|^2 + H^2)^2, \tag{41}$$

(38) can be represented as

$$\frac{\rho_{k,d}}{\beta_{3,k}[s]} \leq 2^{\beta_{1,k}[s]} - 1 \tag{42}$$

We can replace the right sides of (41) and (42) with their first-order Taylor expansions for any given local points $q^r[s]$ and

$$\gamma_0 = \sum_{k=1}^{K} p_k[s]\theta_1[s]\frac{\delta_t}{K} + \eta\left(\sum_{k=1}^{K}\left(p_{k,d}[s]\theta_0[s]\frac{\delta_t}{K} + k_u(f_{k,u}[s])^3\theta_2[s]\delta_t\right) + \frac{\sigma_a^2}{h_a[s]}\left(2^{\frac{\sum_{k=1}^{K}\left(l_{k,rad}[s]+l_{k,off}[s]-l_{k,u}[s]\right)}{B\theta_2[s]\delta_t}} - 1\right)\theta_2[s]\delta_t\right) \tag{22}$$

$$\gamma_1 = \sum_{k=1}^{K} p_k[s]\theta_1[s]\frac{\delta_t}{K} + \eta\left(\sum_{k=1}^{K}\left(p_{k,d}[s]\theta_0[s]\frac{\delta_t}{K} + k_u(f_{k,u}[s])^3\theta_2[s]\delta_t\right) + \frac{\sigma_a^2}{h_a[s]}\left(2^{\frac{\sum_{k=1}^{K}\left(\theta_0[s]\frac{\delta_t}{K}R_{k,rad}^s[s]+l_{k,off}[s]-l_{k,u}[s]\right)}{B\theta_2[s]\delta_t}} - 1\right)\theta_2[s]\delta_t\right) \tag{26}$$

$$\gamma_2 = \sum_{k=1}^{K} p_k[s]\theta_1[s]\frac{\delta_t}{K} + \eta\left(\sum_{k=1}^{K}\left(p_{k,d}[s]\theta_0[s]\frac{\delta_t}{K} + k_u(f_{k,u}[s])^3\theta_2[s]\delta_t\right) + \frac{\sigma_a^2}{h_a[s]}\left(2^{\frac{\sum_{k=1}^{K}\left(l_{k,rad}[s]+\theta_1[s]\frac{\delta_t}{K}R_{k,off}^c[s]-l_{k,u}[s]\right)}{B\theta_2[s]\delta_t}} - 1\right)\theta_2[s]\delta_t\right) \tag{30}$$

$$\gamma_3 = \frac{\sigma_a^2}{h_a[s]}\left(2^{\frac{\sum_{k=1}^{K}\left(\theta_0[s]\frac{\delta_t}{K}B\log_2\left(1+\frac{p_{k,d}[s]h_{k,rad}[s]}{\sigma_u^2}\right)+\theta_1[s]\frac{\delta_t}{K}B\log_2\left(1+\frac{p_k[s]h_k[s]}{\sigma_u^2}\right)-\frac{f_{k,u}[s]}{C_k}\theta_2[s]\delta_t\right)}{B\theta_2[s]\delta_t}} - 1\right)\theta_2[s]\delta_t + P(\|v[s]\|)\delta_t \tag{32}$$

$\beta_{1,k}^r[s]$, which are respectively denoted as

$$\begin{aligned}\xi_{2,k}^r[s] &= \left(\|q^r[s]-u_k\|^2+H^2\right)^2 \\ &+4\left(\|q^r[s]-u_k\|^2+H^2\right)(q^r[s]-u_k)^T(q[s]-q^r[s])\end{aligned} \tag{43}$$

$$\xi_{3,k}^r[s] = 2^{\beta_{1,k}^r[s]}+2^{\beta_{1,k}^r[s]}\ln 2\left(\beta_{1,k}[s]-\beta_{1,k}^r[s]\right) \tag{44}$$

Similarly, by introducing the auxiliary variables $\beta_{4,k}[s], k = 1,2,...,K$, which satisfy

$$\beta_{4,k}[s]-H^2 \le \|q[s]-u_k\|^2 \tag{45}$$

(39) can be represented as

$$\frac{\rho_k}{\beta_{4,k}[s]} \le 2^{\beta_{2,k}[s]}-1 \tag{46}$$

We can replace the right sides of (45) and (46) with their first-order Taylor expansions for any given local points $q^r[s]$ and $\beta_{2,k}^r[s]$, which are respectively denoted as

$$\xi_{4,k}^r[s] = \|q^r[s]-u_k\|^2+2(q^r[s]-u_k)^T(q[s]-q^r[s]) \tag{47}$$

$$\xi_{5,k}^r[s] = 2^{\beta_{2,k}^r[s]}+2^{\beta_{2,k}^r[s]}\ln 2\left(\beta_{2,k}[s]-\beta_{2,k}^r[s]\right) \tag{48}$$

Furthermore, (36b) is non-convex and can be expressed as

$$\|q[s]-u_a\|^2+H^2 \le \frac{\rho_{\max}}{\beta_0[s]-1} \tag{49}$$

We replace the right side of (49) with its first-order Taylor expansion for any given local point $\beta_0^r[s]$, which is denoted as

$$\xi_6^r[s] = \frac{\rho_{\max}}{\beta_0^r[s]-1}-\frac{\rho_{\max}}{\left(\beta_0^r[s]-1\right)^2}\left(\beta_0[s]-\beta_0^r[s]\right) \tag{50}$$

Therefore, the first term of the objective function γ_3 is represented as

$$\begin{aligned}g[s] &= \rho_a[s]\beta_0[s](\|q[s]-u_a\|^2+H^2) \\ &-\rho_a[s](\|q[s]-u_a\|^2+H^2)\end{aligned} \tag{51}$$

where $\rho_a = \frac{\theta_2[s]\delta_t\sigma_a^2}{\beta_{com}}$. By introducing the slack variable $\beta_5[s]$ that satisfies

$$\|q[s]-u_a\|^2 \le \beta_5[s], \tag{52}$$

The upper bound of (51) is represented as

$$\widetilde{g}[s] = \rho_a[s]\beta_0[s]\beta_5[s]-\rho_a[s]\beta_5[s]+\rho_a[s](\beta_0[s]-1)H^2 \tag{53}$$

According to [35], for any given local point $\{\beta_0^r[s],\beta_5^r[s]\}$, $\beta_0[s]\beta_5[s]$ can be replaced by its first-order Taylor expansion, which is denoted as

$$\begin{aligned}\xi_7^r[s] &= \beta_0^r[s]\beta_5[s]+\beta_0[s]\beta_5^r[s]+\tfrac{\kappa}{2}(\beta_0[s]-\beta_0^r[s])^2 \\ &+\tfrac{\kappa}{2}(\beta_5[s]-\beta_5^r[s])^2\end{aligned} \tag{54}$$

where κ is a small positive constant. $R_{k,rad}[s]$ and $R_{k,off}[s]$ in constraint (20b) can be replaced by their first-order Taylor expansions at a given local point $q^r[s]$ as follows

$$\begin{aligned}R_{k,rad}^r[s] &= B\log_2\left(1+\frac{\beta_{rad}p_{k,d}[s]}{\sigma_u^2\left(\|q^r[s]-u_k\|^2+H^2\right)^2}\right) \\ &-\frac{2B\beta_{rad}p_{k,d}[s]\left(\|q[s]-u_k\|^2-\|q^r[s]-u_k\|^2\right)}{\ln 2\left(\sigma_u^2\left(\|q^r[s]-u_k\|^2+H^2\right)^2+\beta_{rad}p_{k,d}[s]\right)\left(\|q^r[s]-u_k\|^2+H^2\right)}\end{aligned} \tag{55}$$

$$\begin{aligned}R_{k,off}^r[s] &= B\log_2\left(1+\frac{\beta_{com}p_k[s]}{\sigma_u^2\left(\|q^r[s]-u_k\|^2+H^2\right)}\right) \\ &-\frac{B\beta_{com}p_k[s]\left(\|q[s]-u_k\|^2-\|q^r[s]-u_k\|^2\right)}{\ln 2\left(\sigma_u^2\left(\|q^r[s]-u_k\|^2+H^2\right)+\beta_{com}p_k[s]\right)\left(\|q^r[s]-u_k\|^2+H^2\right)}\end{aligned} \tag{56}$$

Therefore, the optimization problem (31) is redescribed as

$$\begin{aligned}\min_{q[s],\tau,\beta}\ & \rho_a[s]\xi_7^r[s]-\rho_a[s]\beta_5[s] \\ & +\rho_a[s](\beta_0[s]-1)H^2+P_1(v_1[s])\delta_t\end{aligned} \tag{57a}$$

$$\begin{aligned}\text{s.t.}\quad & \beta_0[s]\ge 1,\beta_{1,k}[s]\ge 0,\beta_{2,k}[s]\ge 0,\beta_{3,k}[s]\ge 0, \\ & \beta_{4,k}[s]\ge 0,\beta_5[s]\ge 0,\forall k\end{aligned} \tag{57b}$$

$$\xi_1^r[s] \ge \frac{1}{\tau_2^2[s]} \tag{57c}$$

$$\beta_{3,k}[s] \le \xi_{2,k}^r[s] \tag{57d}$$

$$\frac{\rho_{k,d}}{\beta_{3,k}[s]}+1 \le \xi_{3,k}^r[s] \tag{57e}$$

$$\beta_{4,k}[s]-H^2 \le \xi_{4,k}^r[s] \tag{57f}$$

$$\frac{\rho_k}{\beta_{4,k}[s]}+1 \le \xi_{5,k}^r[s] \tag{57g}$$

$$\|q[s]-u_a\|^2+H^2 \le \xi_6^r[s] \tag{57h}$$

$$\begin{aligned}&\theta_0[s]\tfrac{\delta_t}{K}R_{k,rad}^r[s]+\theta_1[s]\tfrac{\delta_t}{K}R_{k,off}^r[s] \\ &\ge \tfrac{f_{k,u}[s]}{C_k}\theta_2[s]\delta_t\end{aligned} \tag{57i}$$

$$(20h)-(20j),(33a),(40),(52) \tag{57j}$$

where $\beta = \{\beta_0[s],\beta_{1,k}[s],\beta_{2,k}[s],\beta_{3,k}[s],\beta_{4,k}[s],\beta_5[s]\}$ is the set of auxiliary variables. Problem (57) is convex and can be directly solved using the CVX.

The original optimization problem (20) can be solved by through iteratively optimization the resource allocation optimization subproblem and UAV trajectory optimization subproblem. The joint iterative optimization is shown in Algorithm 2.

Algorithm 2 Joint iterative optimization of resource allocation and UAV trajectory

1: **Initialize**: the iteration index r=0, the resource allocation $\mathbf{L}^r[s] = [f_{k,u}^r[s],p_{k,d}^r[s],p_k^r[s]]$, the UAV trajectory $\mathbf{q}^r[s]$, and the tolerance error ε;
2: **repeat**
3: fixing $\mathbf{q}^r[s]$, solve to get solution $\mathbf{L}^{r+1}[s]$ by Algorithm 1;
4: fixing $\mathbf{L}^{r+1}[s]$, solve (57) to get solution $\mathbf{q}^{r+1}[s]$;
5: $r = r+1$;
6: **until** the target converges within the error of ε;
7: **Output**: the resource allocation $\mathbf{L}[s]$ and the UAV trajectory $\mathbf{q}[s]$.

IV. Numerical Results

In this section, we engage in simulations to confirm the validity of the system model and the efficiency of the optimization approach. The specific parameter configurations for the simulation experiments are presented in Table I. To illustrate

TABLE I
SIMULATION PARAMET

Parameter	Value
total bandwidth	B = 1 MHz
maximum CPU frequency	$f_{u,\max}$ = 5 GHz
CPU cycles per bit	C_k = 1000 cycles/bit
flight altitude	H = 20 M
amount of UEs	K = 6
maximum UE transmit power	$p_{l,\max}$ = 2 W
maximum UAV sensing power	$p_{d,\max}$ = 6 W
maximum UAV transmit power	$p_{u,\max}$ = 2 W
initial UAV location	q_I = (0,0) m
final UAV location	p_F= (40,40) m
maximum flight velocity	$v_{\max}$ = 25 m/s
tip speed of rotor blade	U_{tip} = 120 m/s
mean rotor induced velocity	v_0 = 4.03
air density	ρ_0 =1.225 kg/m^3
rotor disc area	A = 0.503 m^2
fuselage drag ratio	d_0 = 0.6
rotor solidity	s_0 = 0.05
task completion time	T = 5 seconds
time slot number	s = 10
weight	η = 0.1

the superiorities of our proposed scheme, we have devised two benchmark schemes for comparisons. The first scheme is only relaying design: the UAV does not perform computations and can only serve as a relay to offload all task data to the AP. The second scheme is no AP design: the system does not have AP assistance, and all computing tasks are executed by the UAV.

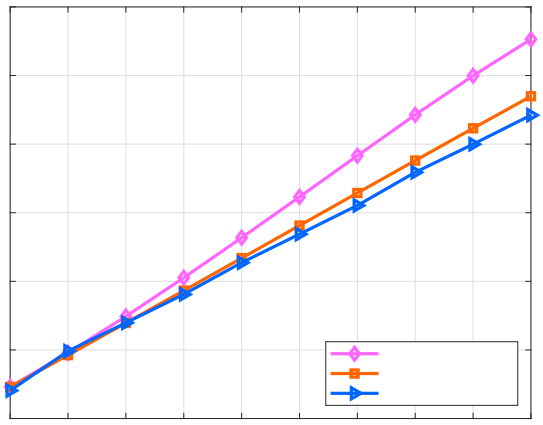

Fig. 3. The weighted total energy consumption versus the flight period T under different schemes.

Fig. 3 shows the weighted total energy consumption versus the flight period T. We can see that the weighted total energy consumption of all three schemes increases as T. For the only relaying design, the UAV does not perform computing, and it offloads all the computing tasks to the AP, thus consuming a large amount of energy. For the no AP design, the UAV also consumes much energy for computing. Therefore, the proposed scheme outperforms the other schemes due to ISCAC design as well as trajectory optimization.

Fig. 4 shows the initial trajectory and velocity of the UAV, as well as the optimized trajectory and velocity of the UAV under different distributions of UEs and AP. From the results of Fig. 4(a), 4(b) and 4(c), it can be seen that the distribution of UEs affects the UAV trajectory. To reduce energy consumption, the UAV is encouraged to fly close to the UEs. In addition, AP coordinates also have a certain impact on the UAV trajectory. Specifically, during the process of offloading to the AP, the UAV adjusts its flight path to approach the AP more closely, aiming to minimize energy consumption. From Fig. 4(d), 4(e) and 4(f), it can be seen that the UAV hovers or flies at a extremely low speed at certain positions. This behavior is attributed to the UAV attaining an advantageous service position within the current time slot. By adopting such a flight pattern, the UAV effectively reduces energy consumption.

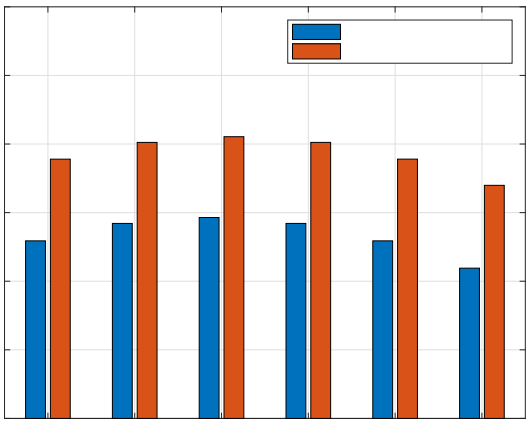

Fig. 5. Radar estimation information rate of each UE.

Fig. 5 illustrates the radar estimation information rate for each UE with both the initial trajectory and the optimized trajectory. It shows that the proposed optimization algorithm is capable of achieving a higher radar estimation information rate compared to the initial trajectory.

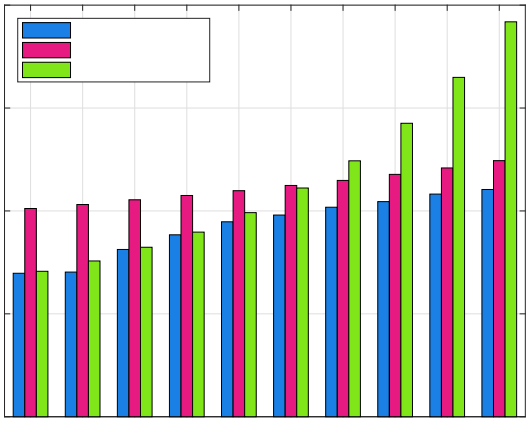

Fig. 6. The weighted total energy consumption versus sum radar estimation rate under different schemes.

Fig. 6 shows the weighted total energy consumption versus

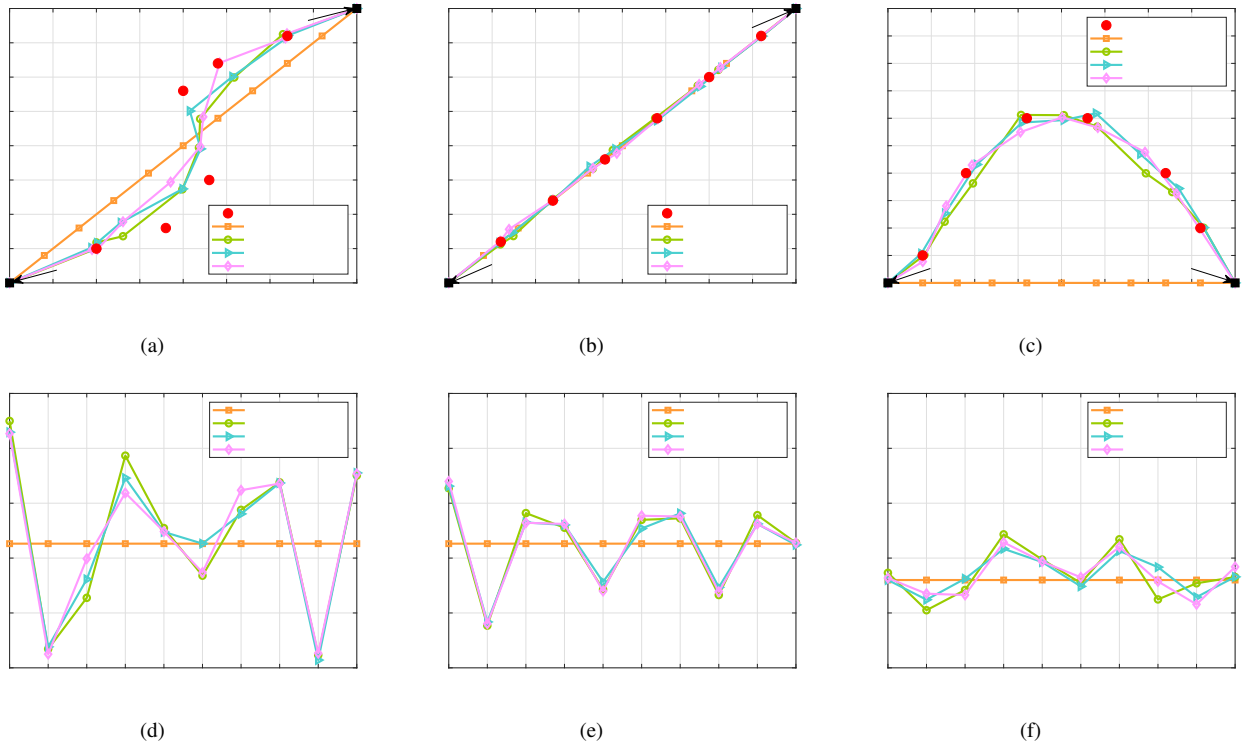

Fig. 4. (a) UAV trajectory with the UEs distribute on both sides of the initial UAV trajectory; (b) UAV trajectory with the UEs uniformly distribute on the initial UAV trajectory; (c) UAV trajectory with the UEs distribute on one side of the initial UAV trajectory; (d) UAV velocity with the UEs distribute on both sides of the initial UAV trajectory; (e) UAV velocity with the UEs uniformly distribute on the initial UAV trajectory; (f) UAV velocity with the UEs distribute on one side of the initial UAV trajectory;

sum radar estimation rate under different schemes. It is seen that the higher the sum radar estimation rate, the greater the sensing energy consumption of the UAV. However, the proposed scheme design requires the least energy consumption. This is because in the no AP design, the energy consumption computed by the UAV itself increases, while in the only relaying design, the UAV energy consumption for offloading tasks to the AP also increases.

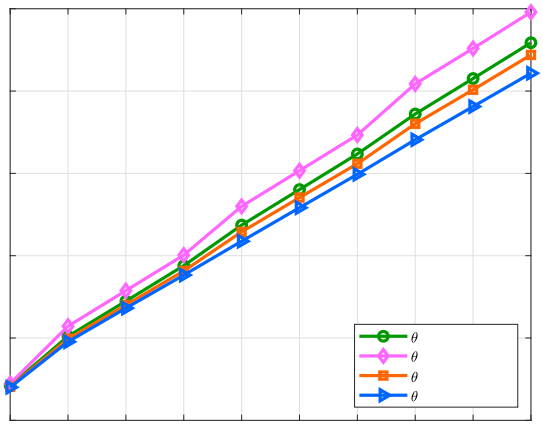

Fig. 7. The weighted total energy consumption versus the period T under different time slot allocations.

Fig. 7 illustrates the weighted total energy consumption under different time slot allocations. We can see that the total energy consumption of each scheme increases as T, but the energy consumption of the average time-slot allocation scheme is the least.

V. CONCLUSIONS

In this paper, we propose a UAV-enabled ISCAC model for IoT, where the UAV senses UEs to acquire radar detection information, executes computing tasks, and offloads incomplete tasks to the AP for further processing. By performing joint optimization of the UAV CPU frequency, UAV radar sensing power, UEs transmit power and UAV trajectory, we aim to minimize the overall energy consumption of both the UAV and UEs. A joint iterative optimization algorithm of resource allocation and UAV trajectory is proposed to obtain the optimal solution for the original problem. The numerical findings provide strong evidence for the effectiveness and superiority of the proposed scheme when compared to the other benchmark schemes.

REFERENCES

[1] K. Chopra, K. Gupta, and A. Lambora, "Future internet: The internet of things-a literature review," in *2019 International Conference on Machine Learning, Big Data, Cloud and Parallel Computing (COMITCon)*, 2019, pp. 135–139.

[2] D. C. Nguyen, M. Ding, P. N. Pathirana, A. Seneviratne, J. Li, D. Niyato, O. Dobre, and H. V. Poor, "6G internet of things: A comprehensive survey," *IEEE Internet of Things Journal*, vol. 9, no. 1, pp. 359–383, 2022.

[3] Y. Zeng, R. Zhang, and T. J. Lim, "Wireless communications with unmanned aerial vehicles: opportunities and challenges," *IEEE Communications Magazine*, vol. 54, no. 5, pp. 36–42, 2016.

[4] Y. Zeng, J. Xu, and R. Zhang, "Energy minimization for wireless communication with rotary-wing UAV," *IEEE Transactions on Wireless Communications*, vol. 18, no. 4, pp. 2329–2345, 2019.

[5] N. Zhao, Y. Li, S. Zhang, Y. Chen, W. Lu, J. Wang, and X. Wang, "Security enhancement for NOMA-UAV networks," *IEEE Transactions on Vehicular Technology*, vol. 69, no. 4, pp. 3994–4005, 2020.

[6] Q. Qi, X. Chen, A. Khalili, C. Zhong, Z. Zhang, and D. W. K. Ng, "Integrating sensing, computing, and communication in 6G wireless networks: Design and optimization," *IEEE Transactions on Communications*, vol. 70, no. 9, pp. 6212–6227, 2022.

[7] J. Mu, R. Zhang, Y. Cui, N. Gao, and X. Jing, "UAV meets integrated sensing and communication: Challenges and future directions," *IEEE Communications Magazine*, vol. 61, no. 5, pp. 62–67, 2023.

[8] K. Meng, Q. Wu, J. Xu, W. Chen, Z. Feng, R. Schober, and A. L. Swindlehurst, "UAV-enabled integrated sensing and communication: Opportunities and challenges," *IEEE Wireless Communications*, 2023, Early Access, doi:10.1109/MWC.131.2200442.

[9] K. Meng, Q. Wu, S. Ma, W. Chen, K. Wang, and J. Li, "Throughput maximization for UAV-enabled integrated periodic sensing and communication," *IEEE Transactions on Wireless Communications*, vol. 22, no. 1, pp. 671–687, 2023.

[10] W. Jiang, A. Wang, Z. Wei, M. Lai, C. Pan, Z. Feng, and J. Liu, "Improve sensing and communication performance of UAV via integrated sensing and communication," in *2021 IEEE 21st International Conference on Communication Technology (ICCT)*, 2021, pp. 644–648.

[11] K. Zhang and C. Shen, "UAV aided integrated sensing and communications," in *2021 IEEE 94th Vehicular Technology Conference (VTC2021-Fall)*, 2021, pp. 1–6.

[12] Z. Wan, Z. Gao, S. Tan, and L. Fang, "Joint channel estimation and radar sensing for UAV networks with mmwave massive MIMO," in *2022 International Wireless Communications and Mobile Computing (IWCMC)*, 2022, pp. 44–49.

[13] J. Zhao, F. Gao, W. Jia, W. Yuan, and W. Jin, "Integrated sensing and communications for UAV communications with jittering effect," *IEEE Wireless Communications Letters*, vol. 12, no. 4, pp. 758–762, 2023.

[14] Z. Lyu, G. Zhu, and J. Xu, "Joint maneuver and beamforming design for UAV-enabled integrated sensing and communication," *IEEE Transactions on Wireless Communications*, vol. 22, no. 4, pp. 2424–2440, 2023.

[15] A. A. Salem, M. H. Ismail, and A. S. Ibrahim, "Active reconfigurable intelligent surface-assisted MISO integrated sensing and communication systems for secure operation," *IEEE Transactions on Vehicular Technology*, vol. 72, no. 4, pp. 4919–4931, 2023.

[16] Y. Liu, S. Liu, X. Liu, Z. Liu, and T. S. Durrani, "Sensing fairness based energy efficiency optimization for UAV enabled integrated sensing and communication," *IEEE Wireless Communications Letters*, vol. 12, no. 10, pp. 1702–1706, 2023.

[17] Z. Ning, Y. Yang, X. Wang, Q. Song, L. Guo, and A. Jamalipour, "Multi-agent deep reinforcement learning based UAV trajectory optimization for differentiated services," *IEEE Transactions on Mobile Computing*, 2023, Early Access, doi:10.1109/TMC.2023.3312276.

[18] Y. Qin, Z. Zhang, X. Li, W. Huangfu, and H. Zhang, "Deep reinforcement learning based resource allocation and trajectory planning in integrated sensing and communications UAV network," *IEEE Transactions on Wireless Communications*, vol. 22, no. 11, pp. 8158–8169, 2023.

[19] Y. Gao, Y. Guo, P. Wang, S. Yang, J. Wang, X. Wang, Y. Ding, W. Lu, Y. Zhang, G. Huang, and J. Cao, "Secure enhancement in NOMA-based UAV-MEC networks," in *IEEE INFOCOM 2022 - IEEE Conference on Computer Communications Workshops (INFOCOM WKSHPS)*, 2022, pp. 1–6.

[20] T. Liu, M. Cui, G. Zhang, Q. Wu, X. Chu, and J. Zhang, "3d trajectory and transmit power optimization for UAV-enabled multi-link relaying systems," *IEEE Transactions on Green Communications and Networking*, vol. 5, no. 1, pp. 392–405, 2021.

[21] D. Wang, J. Tian, H. Zhang, and D. Wu, "Task offloading and trajectory scheduling for UAV-enabled MEC networks: An optimal transport theory perspective," *IEEE Wireless Communications Letters*, vol. 11, no. 1, pp. 150–154, 2022.

[22] M. Li, N. Cheng, J. Gao, Y. Wang, L. Zhao, and X. Shen, "Energy-efficient UAV-assisted mobile edge computing: Resource allocation and trajectory optimization," *IEEE Transactions on Vehicular Technology*, vol. 69, no. 3, pp. 3424–3438, 2020.

[23] X. Zhang, J. Zhang, J. Xiong, L. Zhou, and J. Wei, "Energy-efficient multi-UAV-enabled multiaccess edge computing incorporating NOMA," *IEEE Internet of Things Journal*, vol. 7, no. 6, pp. 5613–5627, 2020.

[24] M. Asim, M. ELAffendi, and A. A. A. El-Latif, "Multi-IRS and multi-UAV-assisted MEC system for 5g/6g networks: Efficient joint trajectory optimization and passive beamforming framework," *IEEE Transactions on Intelligent Transportation Systems*, vol. 24, no. 4, pp. 4553–4564, 2023.

[25] W. Lu, Y. Ding, Y. Feng, G. Huang, N. Zhao, A. Nallanathan, and X. Yang, "Dinkelbach-guided deep reinforcement learning for secure communication in UAV-aided MEC networks," in *GLOBECOM 2022 - 2022 IEEE Global Communications Conference*, 2022, pp. 1740–1745.

[26] T. Zhang, Y. Xu, J. Loo, D. Yang, and L. Xiao, "Joint computation and communication design for UAV-assisted mobile edge computing in IoT," *IEEE Transactions on Industrial Informatics*, vol. 16, no. 8, pp. 5505–5516, 2020.

[27] B. Liu, Y. Wan, F. Zhou, Q. Wu, and R. Q. Hu, "Resource allocation and trajectory design for MISO UAV-assisted MEC networks," *IEEE Transactions on Vehicular Technology*, vol. 71, no. 5, pp. 4933–4948, 2022.

[28] X. Wang, Z. Ning, S. Guo, M. Wen, L. Guo, and H. V. Poor, "Dynamic UAV deployment for differentiated services: A multi-agent imitation learning based approach," *IEEE Transactions on Mobile Computing*, vol. 22, no. 4, pp. 2131–2146, 2023.

[29] N. Huang, C. Dou, Y. Wu, L. Qian, B. Lin, and H. Zhou, "Unmanned aerial vehicle aided integrated sensing and computation with mobile edge computing," *IEEE Internet of Things Journal*, vol. 10, no. 91, pp. 16 830–16 844, 2023.

[30] Y. Xu, T. Zhang, Y. Liu, and D. Yang, "UAV-enabled integrated sensing, computing, and communication: A fundamental trade-off," *IEEE Wireless Communications Letters*, vol. 12, no. 5, pp. 843–847, 2023.

[31] X. Lin, V. Yajnanarayana, S. D. Muruganathan, S. Gao, H. Asplund, H.-L. Maattanen, M. Bergstrom, S. Euler, and Y.-P. E. Wang, "The sky is not the limit: LTE for unmanned aerial vehicles," *IEEE Communications Magazine*, vol. 56, no. 4, pp. 204–210, 2018.

[32] K. Mao, Q. Zhu, Y. Qiu, X. Liu, M. Song, W. Fan, A. B. J. Kokkeler, and Y. Miao, "A UAV-aided real-time channel sounder for highly dynamic nonstationary A2G scenarios," *IEEE Transactions on Instrumentation and Measurement*, vol. 72, pp. 1–15, 2023.

[33] B. Hua, H. Ni, Q. Zhu, C.-X. Wang, T. Zhou, K. Mao, J. Bao, and X. Zhang, "Channel modeling for UAV-to-ground communications with posture variation and fuselage scattering effect," *IEEE Transactions on Communications*, vol. 71, no. 5, pp. 3103–3116, 2023.

[34] C. Zhan and H. Lai, "Energy minimization in internet-of-things system based on rotary-wing UAV," *IEEE Wireless Communications Letters*, vol. 8, no. 5, pp. 1341–1344, 2019.

[35] G. Scutari, F. Facchinei, and L. Lampariello, "Parallel and distributed methods for constrained nonconvex optimization–part i: Theory," *IEEE Transactions on Signal Processing*, vol. 65, no. 8, pp. 1929–1944, 2017.

Yige Zhou received the B.Sc. degree in Communication Engineering from Jilin University, China, in 2022. She is currently working toward the M.Sc. degree with the School of Information and Communication Engineering, Dalian University of Technology, Dalian, China. Her research interests include mobile edge computing, integrated sensing and communication, and communication resource optimization.

Xin Liu (Senior Member, IEEE) received the M.Eng. degree and the Ph.D. degree in Communication Engineering from the Harbin Institute of Technology in 2008 and 2012, respectively. He is currently an Associate Professor with the School of Information and Communication Engineering, Dalian University of Technology, China. From 2012 to 2013, he was a Research Fellow with the School of Electrical and Electronic Engineering, Nanyang Technological University, Singapore. From 2013 to 2016, he was a Lecturer with the College of Astronautics, Nanjing University of Aeronautics and Astronautics, China. His research interests focus on communication signal processing, cognitive radio, spectrum resource allocation, and broadband satellite communications.

Xiangping Zhai (Member, IEEE) is currently an Associate Professor in Computer Engineering with the College of Computer Science and Technology, Nanjing University of Aeronautics and Astronautics, China. He received the B.Eng. degree in Computer Science and Technology from Shandong University in 2006, and the Ph.D. degree in Computer Science from City University of Hong Kong in 2013. Previously, he was a Postdoctoral Fellow at the City University of Hong Kong. His research interests are in the areas of Internet of Things, power control, edge computing, resource optimization and spatial analytics. He has been actively involved in organizing and chairing sessions, and has served as reviewer for several journals and TPC for several international conferences.

Qiuming Zhu (Senior Member, IEEE) received his BS in electronic engineering from Nanjing University of Aeronautics and Astronautics (NUAA), Nanjing, China, in 2002 and his MS and PhD in communication and information system from NUAA in 2005 and 2012, respectively. Since 2021, he has been a professor in the Department of Electronic Information Engineering, NUAA. From Oct. 2016 to Oct. 2017, June 2018 to Aug. 2018 and June 2018 to Aug. 2018, he was also an academic visitor at Heriot Watt University, Edinburgh, U. K. He has authored or coauthored more than 120 articles in refereed journals and conference proceedings and holds over 40 patents. His current research interests include channel sounding, modeling, and emulation for the fifth/sixth generation (5G/6G) mobile communication, vehicle-to-vehicle (V2V) communication and unmanned aerial vehicles (UAV) communication systems.

Tariq S Durrani (Life Fellow, IEEE) is a Full Professor with the University of Strathclyde, Scotland, UK, where he was Deputy Principal of the University from 2000-06. He is Past Vice President of the Royal Society of Edinburgh and the IEEE, Past President of the IEEE Signal Processing Society and the IEEE Engineering Management Society. He has been the General Chair of several flagship international conferences, including IEEE ICASSP-89, Transputers-91, IEEE IEMC-02, European Universities Convention-2006, and IEEE ICC-07. He is a Fellow of the Royal Academy of Engineering, UK, the Royal Society of Edinburgh, UK, the National Academy of Sciences, USA, and the IEEE. His research interests include statistical signal and image processing, technology management, and higher education management.